IMPACTS OF SIMULATED M9 CASCADIA SUBDUCTION ZONE EARTHQUAKES CONSIDERING AMPLIFICATIONS DUE TO THE GEORGIA SEDIMENTARY BASIN ON RC SHEAR WALL BUILDINGS

Preetish Kakoty[1], Sai Mithra Dyaga[1], Carlos Molina Hutt[1]

[1]Department of Civil Engineering, University of British Columbia, Vancouver, BC, Canada

Southwest British Columbia has the potential to experience large-magnitude earthquakes generated by the Cascadia Subduction Zone (CSZ). Buildings in Metro Vancouver are particularly vulnerable to these earthquakes because the region lies above the Georgia sedimentary basin, which can amplify the intensity of ground motions, particularly at medium-to-long periods. Earthquake design provisions in Canada neglect basin amplification and the consequences of accounting for these effects are uncertain. By leveraging a suite of physics-based simulations of M9 CSZ earthquakes, we develop site-specific and period-dependent spectral acceleration basin amplification factors throughout Metro Vancouver. The M9 simulations, which explicitly account for basin amplification for periods greater than 1-second, are benchmarked against the 2016 BC Hydro ground motion model (GMM), which neglects such effects. Outside the basin, empirical and simulated seismic hazard estimates are consistent. However, for sites within the basin and periods in the 1-5 s range, GMMs significantly underestimate the hazard. The proposed basin amplification factors vary as a function of basin depth, reaching a geometric mean value as high as 4.5 at a 2-second period, with respect to a reference site located just outside the basin. We evaluate the impact of the M9 simulations on tall reinforced concrete shear wall buildings, which are predominant in the region, by developing a suite of idealized structural systems that capture the strength and ductility intended by historical seismic design provisions in Canada. Ductility demands and collapse risk conditioned on the occurrence of the M9 simulations were found to exceed those associated with ground motion shaking intensities corresponding to the 975 and 2475-year return periods, far exceeding the ~500-year return period of M9 CSZ earthquakes.

Cascadia subduction zone; M9 simulated ground motions; Deep sedimentary basin effects; Reinforced concrete shear wall buildings.

INTRODUCTION

The Cascadia Subduction Zone (CSZ) megathrust fault lies in the Pacific Northwest region stretching almost 1000 km from Northern Vancouver Island to Northern California. The last known rupture of the CSZ was in 1700 giving rise to a magnitude (M) ~9 earthquake (Hyndman and Rogers, 2010) that produced tremendous shaking and a huge tsunami that swept across the Pacific. Despite evidence of 13 past large M 8-9 earthquakes in the CSZ (i.e., native oral histories and paleo-seismic records) (Atwater et al., 1995), there are no quantitative observations of the ground shaking during these events. How the CSZ will rupture in an inevitable future megathrust earthquake and the influential variability in ground shaking is largely unknown.

A recent study estimated a 14% probability of rupture of the CSZ in the next 50 years (Frankel and Petersen, 2008). Accuracy of predicted earthquake ground motions depends on properly accounting for the earthquake fault rupture, travel path, and local site conditions. Current Ground Motion Models (GMMs) provide earthquake shaking estimates based on past observations of earthquake magnitude, epicentral or rupture distance, and site properties. These empirical models are insufficient to describe the expected ground motions for a future Cascadia megathrust event because the unique geological conditions of the CSZ and its dynamic rupture characteristics prevent direct comparison between a future Cascadia earthquake and past observations in other parts of the world (Chile, Japan, etc.). With advancements in computing, full 3D wave propagation simulations are usurping the use of GMMs for earthquake shaking prediction, especially for medium-to-long period structures (Atwater et al., 1995). For instance, Frankel et al. (2018) produced 30 sets of broadband synthetic seismograms for M9 CSZ earthquakes by combining synthetic seismograms derived from 3D finite-difference simulations with finite-source stochastic synthetics. These 3D simulations, which considered a variety of rupture parameters to determine the range of expected ground motions, are used in this study. This model by Frankel et al. (2018) was shown to accurately reproduce ground motions from the 2003 M8.3 Tokachi-oki (Wirth et al., 2017) and 2010 M8.8 Maule, Chile (Frankel, 2017) earthquakes.

Metro Vancouver lies above the Georgia sedimentary basin. Past studies have shown that recorded motions have spectral accelerations that are larger in deep sedimentary basins than in surrounding locations (Campbell and Bozorgnia, 2014; Choi et al., 2005; Marafi et al., 2017; Morikawa and Fujiwara, 2013). The effects of deep sedimentary basins on ground motion characteristics have also been observed in physics-based simulations of earthquake ground motions (Aagaard et al., 2010; Frankel et al., 2018; Moschetti et al., 2017; Wirth et al., 2018b). In Canada, currently enforced seismic design provisions, i.e., National Building Code of Canada (NBCC) 2015 (NRCC, 2015), do not explicitly account for these effects. Frankel et al.'s (2018) M9 CSZ simulations used a 3D velocity model of the Pacific Northwest (Stephenson et al., 2017), which characterizes the geological profile of the Cascadia region, and thereby explicitly accounts for basin effects for periods greater than 1-second. Based on these simulations, Frankel et al. (2018) estimated spectral acceleration amplification factors of 2-5 in the 1-10 s period range within the Seattle basin. However, the impact of the Georgia sedimentary basin on spectral accelerations has not yet been studied.

Metro Vancouver, located in southwest of British Columbia, is the third largest metropolitan area in Canada. Metro Vancouver is a collection of cities, with the City of Vancouver being the most populous. Among the multi-faceted earthquake risks facing the region, the concentration of tall buildings and infrastructure in this densely populated area raises questions about the risks to life, property, and recovery from large earthquakes. Although tall buildings are not the only structures at risk, they are of special concern due to their susceptibility to long-period ground motions, which are characteristic of large magnitude subduction earthquakes. Furthermore, the existing tall building stock in the region includes a large number of seismically vulnerable pre-1980 reinforced concrete (RC) shear wall buildings (Yathon et al., 2017). The vulnerability of these structures is compounded by sedimentary basin amplification, which can increase the intensity of earthquake ground motions at medium-to-long periods and the resulting damage in tall structures (Marafi et al., 2019, Bijelić et al,. 2019, Kourehpaz et al., 2020).

This paper benchmarks a suite of simulations of a M9 CSZ earthquake in Metro Vancouver, which explicitly account for basin amplification, against GMMs, i.e., BC Hydro (Abrahamson et al., 2016), which neglect such effects. The M9 simulations are also benchmarked against probabilistic estimates of the hazard from NBCC 2015, namely the 2%, 5%, 10% and 40% in 50-year hazard levels. The evaluations are carried out in strategic locations within and outside of the Georgia sedimentary basin to quantify the effects of the basin on ground motion amplification. Site-specific and period-dependent spectral acceleration basin amplification factors are proposed. These factors are intended to enable explicit consideration of these effects within Canada's 2015 National Seismic Hazard Model (CSHM) for interface source contributions, and associated seismic design provisions. This paper also quantifies the impact of the M9 simulations on tall (>8 stories) reinforced concrete shear wall buildings, which are predominant in Metro Vancouver, by developing a suite of idealized structural systems that capture the strength and ductility intended by historical seismic design provisions in Canada.

OVERVIEW OF SIMULATED M9 CSZ EARTHQUAKES AND GEORGIA SEDIMENTARY BASIN

To better characterize the impact of a megathrust earthquake in the Cascadia corridor, a collaborative group of researchers from the United States Geological Survey (USGS) and University of Washington (UW) developed a suite of 30 simulated M9 CSZ ground motions (Frankel et al., 2018). Each of the 30 scenarios accounts for variations in hypocenter location, extent of the rupture plane and rupture direction. The simulated ground motions were generated using a finite-difference method, for periods greater than 1 s, by utilizing a 3D velocity model (Stephenson et al., 2017). The geological profile of the Georgia sedimentary basin, as developed by Molnar et al. (2014a), was integrated into this velocity model (Stephenson et al., 2017). Therefore, the effects of basin amplification due to the Georgia basin are explicitly accounted for within this suite of simulated M9 CSZ earthquakes. For periods less than 1 s, a stochastic procedure was implemented to generate the ground motions assuming a constant geological profile (Marafi et al., 2019). Therefore, the impacts of the basin on the ground motions is not considered for periods below 1 s. Basin amplification in the 0-1s period range has not been generally been observed in recorded motions (Wirth et al., 2018). The simulated motions were generated assuming a constant time-averaged 30 m shear-wave velocity (V_{s30}) equal to 600 m/s. Hence, these ground motion simulations are representative at sites with dense soils consistent with NEHRP Site Class C (360 m/s $< V_{s30} <$ 760 m/s) (NEHRP, 2003), but may under-predict shaking in softer sites, and over-predict shaking in stiffer sites.

The Georgia sedimentary basin in southwest British Columbia is one in a series of basins in the Pacific Northwest region (England and Bustin, 1998). Based on observed amplification in recorded motions in regions with sedimentary basins (Campillo et al., 1988; Frankel et al., 2009; Olsen, 2000), it is expected that ground motions in Metro Vancouver will also experience ground motion amplification due to the presence of the Georgia basin. The amplifications are likely to occur in the medium-to-long period range and can have adverse consequences on the seismic performance of structures, particularly with periods in the 1-5 s range. Previous studies have estimated average peak ground velocity (*PGV*) basin amplification factors in the Georgia basin of 4.1 and 3.1 for shallow blind-thrust North America plate and deep Juan de Fuca plate scenario earthquakes, respectively (Molnar et al., 2014a, 2014b).

Numerous studies have proposed depth to soils with a shear wave velocity of 1.0, 1.5 and 2.5 km/s, denoted as $Z_{1.0}$, $Z_{1.5}$ and $Z_{2.5}$, as a proxy for deep sedimentary basin depth (Day et al., 2008). However, more recent studies recommend the use of $Z_{2.5}$ for computing basin amplification in the Pacific Northwest as sites with a shallow $Z_{1.0}$ value can still have a deep $Z_{2.5}$ value (Wirth et al., 2018a). Figure 1a shows the variations in $Z_{2.5}$ in southwest British Columbia, with maximum $Z_{2.5}$ values of approximately 4 km. It can be inferred from Figure 1a that Victoria, denoted REF-A, is well outside the basin with a $Z_{2.5}$ value of 0.06 km. West Vancouver, denoted REF-B, is immediately outside the basin boundary with a $Z_{2.5}$ value of 0.67 km, whereas other cities within Metro Vancouver have a range of basin depths. As a result, seven different sites were strategically selected considering their high concentration of building infrastructure, i.e., major urban centers, and a variety of basin depths. Table 1 summarizes the selected locations and their corresponding latitude, longitude, V_{s30}, $Z_{1.0}$ and $Z_{2.5}$, as well as the labels used to locate these sites in Figure 1 and additional maps discussed later. Additionally, depth to primary wave velocity (V_P) of 5.5 km/s is also shown in Table 1 as the depth to bedrock at the sites of interest.

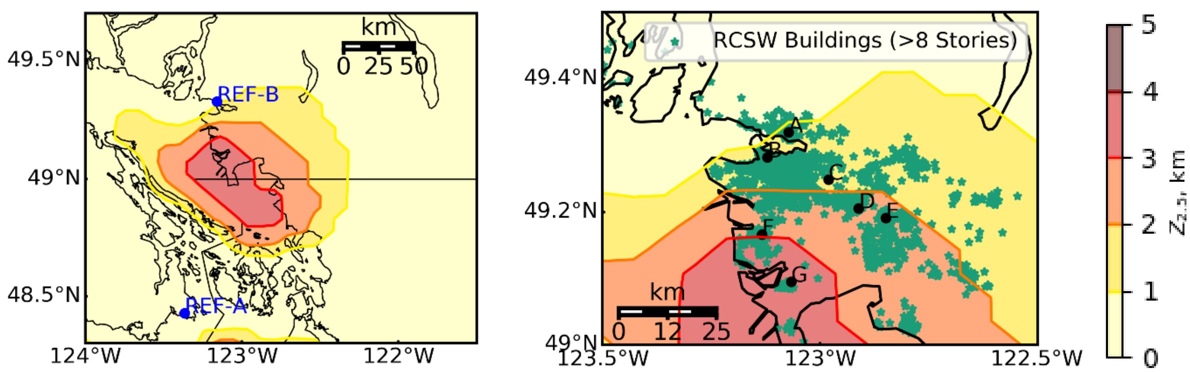

(a) **(b)**

Figure 1. Variations of $Z_{2.5}$ in (a) southwest British Columbia and (b) Metro Vancouver with selected locations including Victoria (REF-A), West Vancouver (REF-B), North Vancouver (A), Vancouver (B), Burnaby (C), New Westminster (D), Surrey (E), Richmond (F) and Delta (G), as well as the geographical distribution of reinforced concrete shear wall (RCSW) buildings (> 8 stories).

Figures 2a and 2b show ground motion acceleration time histories (east-west components) and corresponding geomean response spectra, at the selected locations for one of the simulated M9 CSZ earthquakes considered in the study. The accelerograms in Figure 2a reveal the closer epicentral distance of the scenario to Victoria than locations within Metro Vancouver (earlier arrival time). Figure 2b clearly illustrates that spectral accelerations are significantly higher in locations within Metro Vancouver with higher $Z_{2.5}$ values, e.g., Delta. Because the M9 simulations assume a constant V_{s30} profile of 600 m/s, at sites with softer soils, namely Delta and Richmond, additional amplification is expected. However, in this study, a uniform V_{s30} profile is assumed across all sites.

Table 1. V_{s30}, $Z_{1.0}$, $Z_{2.5}$ and depth to bedrock for selected locations within Metro Vancouver.

Locations	Labels	Latitude (°)	Longitude (°)	V_{s30} (m/s)[1,2]	$Z_{1.0}$ (m)[3]	$Z_{2.5}$ (km)[3]	*Depth to Bedrock (km)*[3]
Victoria	REF-A	48.43	-123.36	360-760	0	0.06	0.85
West Vancouver	REF-B	49.33	-123.16	360-760	120	0.67	3.16
North Vancouver	A	49.32	-123.07	360-760	129	1.18	3.67
Vancouver	B	49.28	-123.12	360-760	133	1.22	3.78
Burnaby	C	49.25	-122.98	360-760	145	1.74	4.51
New Westminster	D	49.21	-122.91	360-760	150	2.23	4.99
Surrey	E	49.19	-122.85	180-360	150	2.23	5.10
Richmond	F	49.17	-123.13	180-360	169	3.22	4.90
Delta	G	49.09	-123.03	180-360	163	3.27	5.49

[1]VC Structural Dynamics LTD. (2016); [2]Monahan (2005); [3]Stephenson et al. (2017).

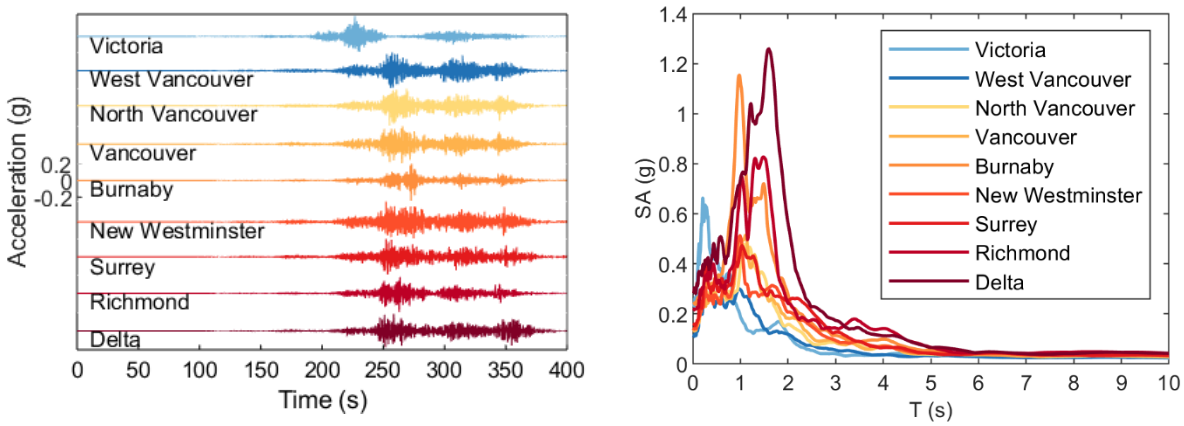

(a) (b)

Figure 2. Sample M9 CSZ earthquake scenario (a) ground motion acceleration time histories (east-west component) and (b) corresponding geomean response spectra at selected locations within Metro Vancouver.

BENCHMARKING SIMULATED VS EMPIRICAL SEISMIC HAZARD CHARACTERIZATIONS

In its design provisions, NBCC 2015 uses a site-specific 5% damped elastic spectrum with a 2% probability of exceedance in 50 years, i.e., a 2475-year return period, to characterize seismic demands for building design. The response spectrum is primarily derived from probabilistic seismic hazard analysis. CSHM 2015 (Adams et al., 2015) includes a range of GMMs for different earthquake sources, including BC Hydro (Abrahamson et al., 2016; BC Hydro, 2012) for subduction earthquakes. To quantify deep basin amplification on ground motion shaking, the response spectra of the suite of simulated M9 CSZ earthquakes are benchmarked against estimates of the BC Hydro GMM for the same set of rupture scenarios. Figures 3a-3i provide a comparison of the average of the geomean spectra for the suite of M9 simulations against corresponding BC Hydro estimates. These spectra are shown for each of the sites presented in Table 1. Additionally, Uniform Hazard Spectra (UHS) with a 2%, 5%, 10% and 40% probability of exceedance in 50 years, as derived from CSHM 2015, are also provided to benchmark the M9 CSZ earthquake scenarios against probabilistic estimates of the hazard.

As seen in Figure 3a, for sites outside of the Georgia basin, i.e., Victoria, the M9 simulations and BC Hydro predictions match well. However, at the basin edge and for sites within the basin, the simulated M9 spectra are significantly higher than the corresponding BC Hydro estimates, particularly in the 1-5 s period range. As observed in Figures 3c-3i, the ratio of the M9 to BC Hydro spectral accelerations in this range strongly correlates with $Z_{2.5}$. At sites with lower $Z_{2.5}$ values, i.e., 1.18 km in North Vancouver, this ratio is approximately 2.7 at a 2 s period. At sites with higher $Z_{2.5}$, i.e., 3.26 km in Delta, the ratio is around 6.2 at the same period.

For locations within the basin with a $Z_{2.5}$ in the range of 1-2 km, e.g., Vancouver, simulated M9 spectral accelerations for periods in the range of 1-3 s are consistent with NBCC 2015 probabilistic seismic hazard estimates with a 975-year return period. For locations within the basin with a $Z_{2.5}$ in the range of 3-4 km, e.g., Richmond, M9 estimates exceed the 2475-year return period probabilistic estimate of the hazard. NBCC 2015 UHS represents contributions to the hazard from all seismic sources in the region, i.e., crustal, intraslab and interface. Therefore, the M9 CSZ earthquake spectra, which has an estimated 500-year return period (Atwater and Hemphill-Haley, 1997), should fall below the 10% in 50-year probabilistic estimate of the hazard. While this observation holds true outside of the basin, i.e., Victoria, the M9 spectra for sites within the basin far exceed this hazard level. For a site just outside the basin, i.e., West Vancouver, the M9 spectra do not follow the BC Hydro estimates in the 1-3 s period, but fall within the 10% in 50-year probabilistic estimate of the hazard.

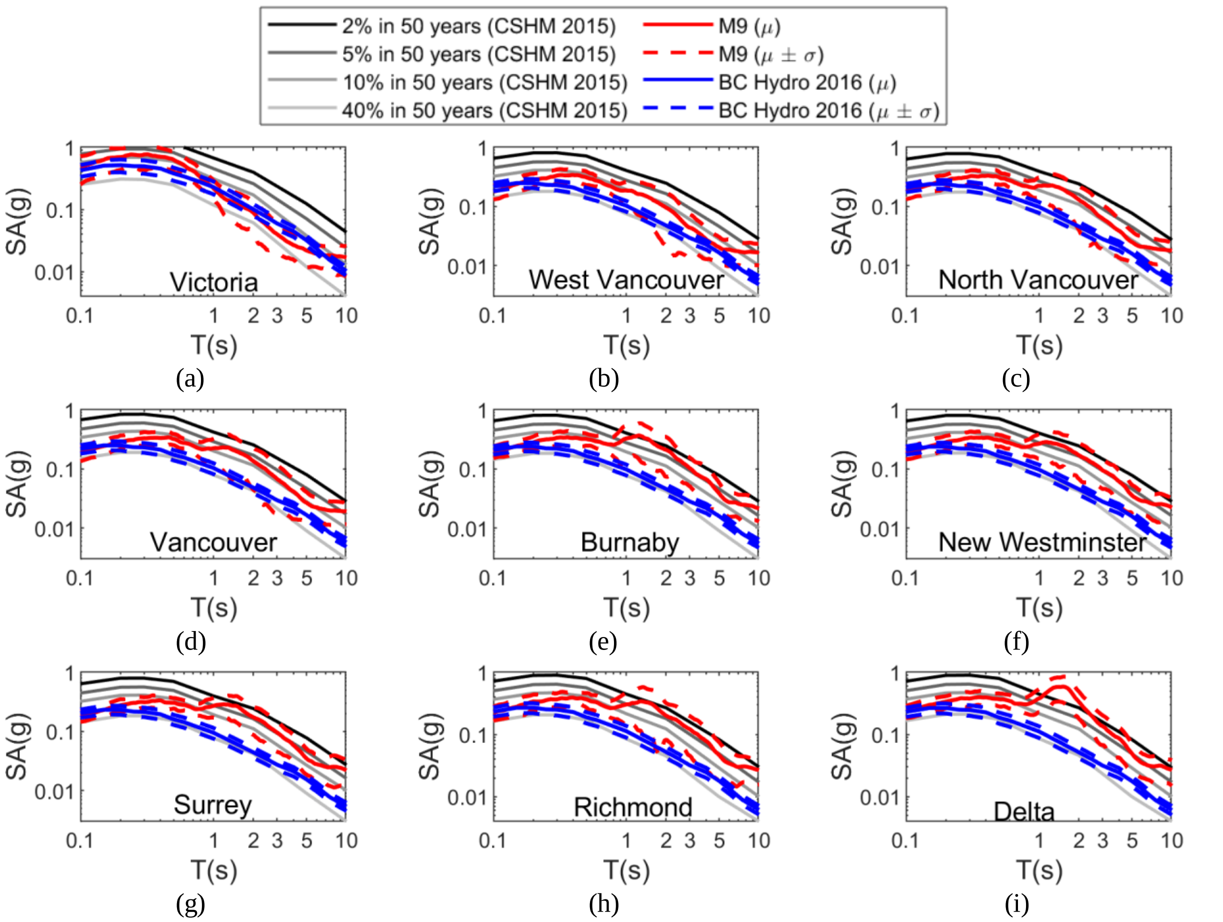

Figure 3. Average response spectra of simulated M9 CSZ earthquake ground motions, BC Hydro estimates and NBCC 2015 probabilistic estimates of the hazard with 2%, 5%, 10% and 40% probability of exceedance in 50 years in (a) Victoria, (b) West Vancouver, (c) North Vancouver, (d) Vancouver, (e) Burnaby, (f) New Westminster, (g) Surrey, (h) Richmond and (i) Delta.

The bias in spectral acceleration for periods between 0.5 and 1 s in the M9 simulations relative to the BC Hydro predictions, as observed in Figure 3, is due to the deterministic portion of the ground motion leaking spectral acceleration intensity at shorter periods, i.e., leaking intensity into the stochastic portion of the ground motion (N. Marafi, personal communication, 2020). This is a limitation the M9 simulations and a future area of research. Many physics-based modellers are now starting to use velocity models that (1) go to a finer resolution, (2) use more efficient codes, (3) and use computers that are able to simulate ground motions for periods of 0.1 s and above, e.g. (Bielak et al., 2016).

SPECTRAL ACCELERATION BASIN AMPLIFICATION FACTORS IN METRO VANCOUVER

In order to accurately quantify the effects of the Georgia sedimentary basins on ground motion shaking in Metro Vancouver, we utilize a site-specific and period-dependent spectral acceleration basin amplification factor, BAF_T^i. For each rupture scenario, site and period, the ratio of the spectral acceleration predicted by the M9 simulations to BC Hydro predictions is computed. This value is then normalized by the same ratio computed at a reference site outside the basin, i.e., Victoria and West Vancouver (REF-A and REF-B in Figure 1a, respectively). The resulting BAF_T^i is the geometric mean of individual basin amplification factors calculated for each rupture scenario. This basin amplification factor, defined in Eq. (1), can be used in current design provisions to amplify design spectral accelerations as a proxy to account for basin effects. This formulation is similar to that proposed by Marafi et al. (2019) but is adjusted in this study to develop site-specific factors.

$$BAF_T^i = \prod_{x=1}^{n} \left(\left(\frac{SA_{M9}^{i,x}(T)}{SA_{GMM}^{i,x}(T)} \right) \Big/ \left(\frac{SA_{M9}^{ref,x}(T)}{SA_{GMM}^{ref,x}(T)} \right) \right)^{1/n} \tag{1}$$

Where BAF_T^i is the spectral acceleration basin amplification factor at a site i and period T, $SA_{M9}^{i,x}$ is the spectral acceleration of the simulated M9 ground motion at period T for a particular site i and rupture scenario x , and $SA_{GMM}^{i,x}$ is the BC Hydro prediction of spectral acceleration at period T for the same site and rupture scenario. $SA_{M9}^{ref,x}$ and $SA_{GMM}^{ref,x}$ represent the same parameters, but calculated at the reference sites outside the basin, and n is the number of rupture scenarios.

Figures 4a and 4b show the BAF_T^i at the sites of interest within Metro Vancouver, listed in Table 1, for a period range of 0.5-10 s, considering both Victoria ($Z_{2.5}$ = 0.06 km) and West Vancouver ($Z_{2.5}$ = 0.67 km) as reference sites. BAF_T^i is computed at 900 equally spaced points (~1.5 km grid) within the region and the resulting geospatial variation is illustrated in Figures 5a and 5b. *BAF*s are highest in the period range of 1-5 s, and remain fairly constant from periods of 5-10 s. Amplification factors are highest in Delta, where the Georgia basin has a $Z_{2.5}$ value of 3.27 km, reaching values of 9.2 at a period of 2 s.

The amplifications computed in this study are substantially higher than those predicted for crustal earthquakes by Campbell and Bozorgnia (2014). In the latter GMM for crustal sources, the basin amplification is equal to 1.0 for $Z_{2.5}$ ranging from 1-3 km. However, if this relationship were applied to the subduction sources and the Georgia basin, it would considerably underestimate the effects of basin amplification illustrated in Figures 4 and 5. Studies that used the M9 simulations to estimate basin amplification in the Seattle basin (Marafi et al., 2019; Wirth et al., 2018a) also found that the Campbell and Bozorgnia (2014) basin term underestimated amplification of spectral accelerations. Frankel et al. (2018) showed that amplification factors from the M9 simulations and ground motion recordings (from earthquakes with similar depths and azimuths as a megathrust event) yielded consistent amplification factors that were significantly higher than those predicted by Campbell and Bozorgnia (2014). These differences are partly attributed to some of the basin amplification being absorbed in the V_{S30} term in NGA-West2 database (Ancheta et al., 2014), used to develop the Campbell and Bozorgnia (2014) basin term, which would not apply to the Seattle basin or the Georgia basin because V_{S30} is similar for sites inside and outside the basin (Wirth et al., 2018a). Basin amplification is dependent on certain properties of the earthquake source, but not others. For example, it appears to be largely independent of the earthquake magnitude and distance from the basin (Wirth et al. 2018). However, basin amplification is highly dependent on the earthquake location and depth, which impacts the azimuth and incidence angle of incoming seismic energy as it enters the basin. Basin amplification has also been shown to be source mechanism dependent both through observations (Thompson et al., 2020) and modeling (Wirth et al., 2019). These effects can be captured through more refined velocity models supported by microzoning studies (Faccioli et al., 2010).

As seen in Figures 4 and 5, *BAF* is sensitive to the choice of reference site, primarily due to the differences in $Z_{2.5}$ between Victoria (0.06 km) and West Vancouver (0.67 km), but possibly also due to the influence of basin-edge effects affecting the West Vancouver site (Molnar et al., 2014b). For instance, Delta has a *BAF* of around 9.2 at a 2 s period with Victoria as the reference site. However, *BAF* is around 4.5 at the same period with West Vancouver as the reference site. In a recent USGS report (Wirth et al., 2018a), it is noted that in order to develop site-specific basin terms using 3D simulations or observations and a reference GMM, a reference $Z_{2.5}$ or shear wave velocity profile, V_S, from the GMM dataset is required. While this information is not currently available, a reference $Z_{2.5}$ and V_S profile of the BC Hydro GMM will permit a more appropriate selection of a reference site to quantify basin amplification in Metro Vancouver. The selection of two reference sites in this study, one on the edge of the sedimentary basin (i.e., West Vancouver) and another farther away from the basin (i.e., Victoria) provides insights into the variability in the amplification estimates and introduces reasonable bounds to the anticipated basin amplification factors in the Metro Vancouver region. To understand the correlation between the basin depth indicator $Z_{2.5}$ and the proposed *BAF*, a regression analysis is carried out with the corresponding values from the seven selected locations within the Georgia basin. Figure 6 shows there is strong correlation between $Z_{2.5}$ and the proposed *BAF*, with stronger correlation at longer periods. While the results in Figure 6 are shown taking Victoria as the reference site, the results are identical if selecting West Vancouver as the reference site.

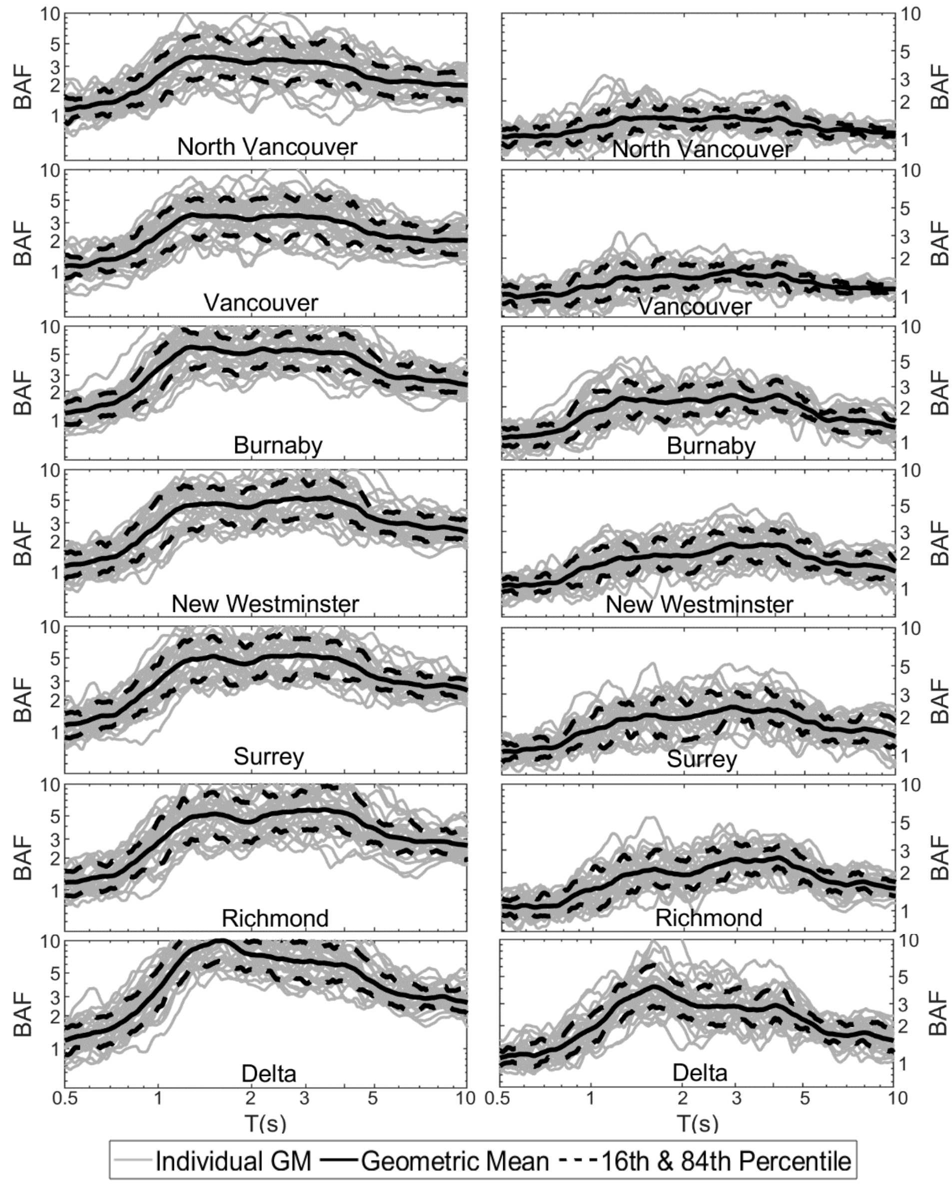

Figure 4: Spectral acceleration Basin Amplification Factors (*BAF*) for selected locations in Metro Vancouver with (a) Victoria and (b) West Vancouver as reference sites.

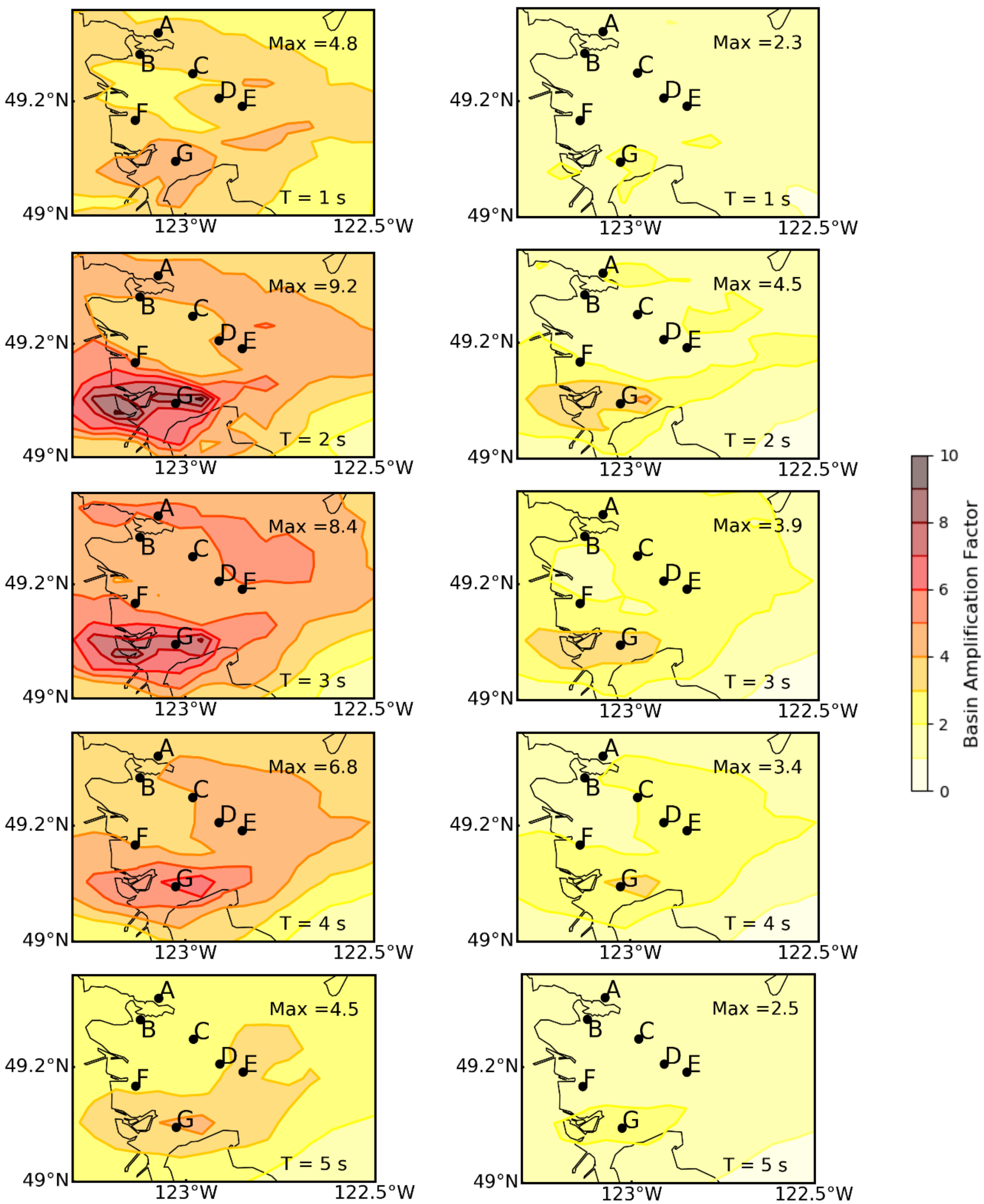

(a) (b)

Figure 5. Geospatial variation of Basin Amplification Factors (*BAF*) within Metro Vancouver for periods of 1, 2, 3, 4 and 5 s (annotated with the maximum *BAF* in the region at the upper-right corner and period at lower-right corner) with (a) Victoria and (b) West Vancouver as reference sites.

Currently enforced basin amplification factors in the city of Seattle (Chang et al., 2014) for performance-based seismic design projects, require amplification factors of 1-2 for periods in the range 0-2 s, and amplification factors of 2 for periods greater than 2 s. These observations were derived from the selection of a reference site immediately outside the Seattle basin. Similar basin amplification factors are reported in this study when using a reference site immediately outside the basin, i.e., West Vancouver (REF-B in Figure 1a).

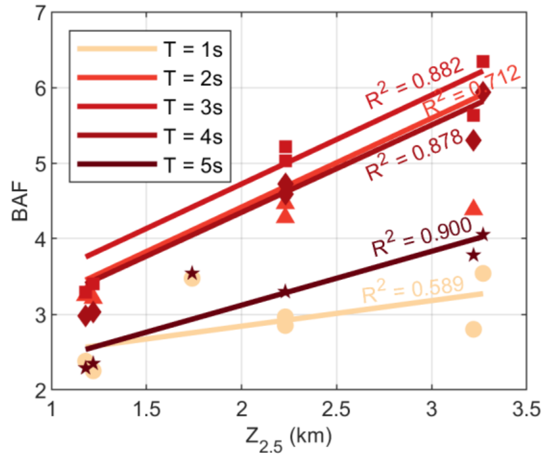

Figure 6. Correlation between $Z_{2.5}$ and the proposed Basin Amplification Factor (*BAF*) in Metro Vancouver.

IDEALIZED RC SHEAR WALL STRUCTURAL ANALYSIS MODELS

Reinforced concrete is the primary construction material for tall buildings in Metro Vancouver. The majority of these buildings employ reinforced concrete shear walls (RCSW) as their lateral force-resisting system (Adebar et al., 2017). While RCSWs have been predominant for tall building construction in many western North American cities since the early 2000s (ATC, 2018; Kakoty et al., 2019), these were also predominant in western Canada since the 1960s. This is in sharp contrast to western US cities, e.g., San Francisco, which primarily adopted a steel moment-resisting frame configuration in the design of tall buildings from the 1960s to the mid-1990s (Molina Hutt et al., 2016, 2019).

There are over 3000 tall (>8 stories) RCSW buildings in Metro Vancouver that lie above the Georgia basin, as can be seen in Figure 1b, which shows the geographical distribution of these buildings overlaying the $Z_{2.5}$ contours discussed earlier, and the sites of interest used in this study. These buildings were identified within a regional exposure dataset developed by Natural Resources Canada (Natural Resources Canada, Personal Communication, 2019). Tall building data compiled from Emporis (2020) for the City of Vancouver, as shown in Figure 7a, suggests that concrete is the predominant material of construction for buildings taller than 8 stories, constituting 90% of a total 752 buildings identified. Based on the evolution of NBCC seismic design requirements and the construction of concrete buildings dating back to the 1950s, we introduce qualitative descriptors of the anticipated seismic performance provided by different building codes in relation to modern design requirements, namely pre-code (PC), low code (LC), moderate code (MC) and high code (HC) as seen in Figure 7. This classification is consistent with past (ARUP, 2017; Journeay et al., 2015) and present (City of Vancouver, Personal Communication, 2020) seismic risk studies in the region. Figure 7b shows the number of stories above grade for the tall concrete buildings identified in Figure 7a according to these code eras. As seen in Figure 7b, buildings in the 10-20 story range are predominant. However, the number of buildings of 20 stories and above is also significant. Three of the buildings identified in Figure 7a have more than 50 stories and are not shown in Figure 7b. A related database compiled by Yathon et al. (2017) identified over 300 pre-1980 RCSW buildings in the City of Vancouver in the 7-38 story range with periods ranging from 0.5-5.5 s.

To quantify the seismic demands and collapse risk in the these buildings due to simulated M9 CSZ earthquakes and basin amplification, a series of single degree of freedom (SDOF) systems are developed to capture the salient features intended by historical seismic design provisions in Canada. Changes to the seismic and other design requirements that have been introduced in NBCC over the past 80 years offer important clues to appraise the anticipated seismic performance of existing buildings in Canada. To capture important changes in the evolution of the building code, the SDOF models are idealized and calibrated to represent four distinct versions of NBCC, namely the 1965, 1985, 1995 and 2015 editions, shown in bold in Figure 7a. These idealized systems are used to benchmark M9 demands against demands from probabilistic estimates of hazard per CSHM 2015, i.e., 2%, 5%, 10% and 40% probability of exceedance in 50-years. While these simplified systems are not able to fully characterize the unique dynamic characteristics of tall buildings, they provide a general understanding of the anticipated seismic performance in these structures.

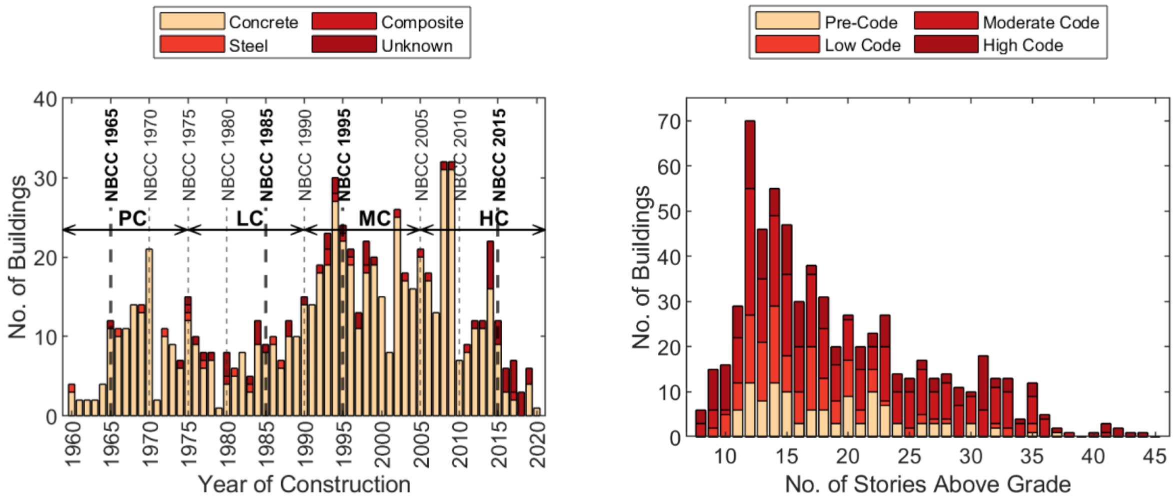

(a) (b)

Figure 7. Distribution of tall buildings (>8 storeys) in the City of Vancouver according to (a) year and material of construction, and (b) number of stories above grade and generalized construction era (for concrete buildings only).

Design Criteria

The idealized RCSW systems are developed to capture significant variations in height with fundamental periods ranging from 1-5 s, in 1-second increments, for NBCC 1965, 1985, 1995 and 2015. The design base shear is estimated from the formulation in each of the code editions considered. A typical seismic weight per story, W, which includes self-weight and superimposed dead load, is assumed to be 45,000 kg (CAC, 2016) in the design base shear calculations. In estimating the total seismic weight of each building, we assume the number of stories is equal to $10 \times T$, where T is the period of the building under consideration in seconds.

In NBCC 1965, the design base shear is calculated per Eq. 2, where V_{1965} represents the design base shear, R_S is the seismic regionalization factor, with a value of 4 for southwestern British Columbia, and C represents type of construction with a value of 0.75 for RCSW buildings. I is the importance factor with a value of 1.0 for a regular building, F is the foundation factor with a value of 1.0 for compressible soils (i.e., not rock) and S is the structural flexibility factor of $0.25/(N+9)$ where N is the number of stories. W represents the seismic weight of the building. Therefore, the design base shear for a 10-story building is equal to 177 kN.

$$V_{1965} = R_S CIFSW \tag{2}$$

The base shear formulation in NBCC 1985 is given by Eq. 3, where v is the velocity zonal factor, which takes a value of 0.25 from the corresponding seismic hazard map, and S_R is the seismic response factor, which is a function of the period of the building, T. For the range of periods considered in this study, S_R is calculated as $0.22/T^{½}$. K represents different types of construction and takes a value of 1.0 for RCSWs. Therefore, for a 10-story building with a 1-second period, S_R takes a value of 0.22, and the resulting base shear is equal to 247 kN.

$$V_{1985} = vS_R KIFW \tag{3}$$

In NBCC 1995, the design base shear is calculated per Eq. 4, where U is a calibration factor with a value of 0.6, consistent with Mitchell et al. (2010). v is the velocity zonal ratio, which takes a value of 0.25 from the corresponding seismic hazard map. S is the seismic response factor, calculated as $1.5/T^{½}$ where T is the period of the building. R factor for ductile wall systems is 4.0. Therefore, the design base shear per NBCC 1995 for a 10-story building is equal to 253 kN.

$$V_{1995} = U(\nu SIFW)/R \tag{4}$$

The base shear formulation in NBCC 2015 is given by Eq. 5, where, $S(T_a)$ is the spectral acceleration at fundamental period of the building, T_a, which, at a 1-second period, takes a value of 0.42g in Vancouver. M_v is the higher mode factor, which takes a value of 1.0 for a 10-story building. R_d is the reduction factor for ductility and R_o is the force modification factor for overstrength, which for ductile RCSWs take values of 4.0 and 1.7, respectively. Therefore, the resulting design base shear for a 10-story per NBCC 2015 is equal to 279 kN.

$$V_{2015} = \frac{S(T_a)M_v IW}{R_d R_o} \tag{5}$$

Figure 8 shows the normalized design base shear (V/W), which is the ratio between the design base shear and the seismic weight of the structure, of all idealized systems considered in this study. The normalized design base shear per NBCC 1965 is the lowest of the four code editions studied, and it decreases significantly for higher periods taking a value as low as 1.3% at a 5-second period. Although, the normalized design base shear is similar for NBCC 1985 and NBCC 1995, there are considerable differences in terms of ductility. The assumed ductility levels (μ) for the different NBCC editions considered are summarized in Table 2. While NBCC 1965 and 1985 did not explicitly consider ductility in the design base shear estimates, the 1995 and 2015 editions include ductility-dependent force reduction factors. As outlined in Mitchell et al. (2010), nominal ductility levels are assumed for the models calibrated to NBCC 1965 and 1985, whereas code-prescribed ductility values are assumed for NBCC 1995 and 2015 designs.

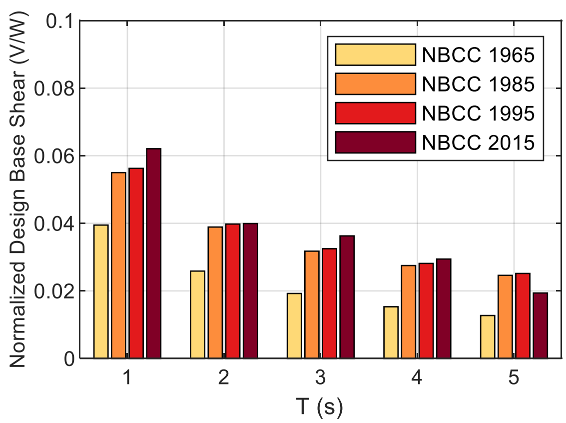

Figure 8. Normalized design base shear of idealized systems at different periods and code eras.

Modeling Assumptions

Idealized SDOF nonlinear models are developed in Openseespy (Zhu et al., 2018) with the Modified Ibarra-Medina-Krawlinker pinching spring material model (Ibarra et al., 2005). This material model captures the both strength and stiffness degradation. The initial stiffness (k) is a function of the period (T) of the structure, and its assumed mass. The yield strength (F_y) is obtained by scaling the design base shear estimates, from Eq. 2-5, by appropriate overstrength factors as outlined in Table 2. Overstrength factors for NBCC 1995 and 2015 are as outlined in the code guidelines. However, for NBCC 1965 and 1985, the overstrength factors, which weren't explicitly addressed in the code, are assumed to be consistent with conventional shear wall construction (NRCC, 2015) as outlined in Table 2. The yielding displacement (δ_y) is a function of the F_y and k. A constant post-yield stiffness equal to 5% of initial stiffness is assumed for all the models and the ultimate strength (F_u) is achieved at the ultimate displacement (δ_u), computed as $\mu \times \delta_y$. The residual strength (F_r) of the systems is assumed to be 20% of F_y. The backbone deteriorates after reaching ultimate strength at rate α_{PC}, which is outlined in Table 2 for the different code eras. 5% Rayleigh damping is assumed in all models.

Table 2. Ductility, overstrength factor and post-capping stiffness degradation coefficients assumed for different code eras.

Variable	NBCC 1965	NBCC 1985	NBCC 1995	NBCC 2015
Ductility (μ)	1.5	1.5	4	4
Overstrength Factor (R_o)	1.3	1.3	1.7	1.7
Post-capping Stiffness Degradation Coefficient (α_{PC})	0.5	0.5	0.1	0.1

The critical points of the monotonic backbones for each idealized system are summarized in Table 3 for variations in structural period and code era. The cyclic deterioration parameters of the material model, controlling strength deterioration (λ_S) and post-capping strength deterioration (λ_C) are assumed to be 20. The cyclic deterioration parameters controlling accelerated reloading stiffness (λ_A) and unloading stiffness deterioration (λ_K) are assumed to be 10. The hysteresis response of the SDOF systems was calibrated to follow those of laboratory tests of RC shear walls subjected to cyclic loading (Kolozvari et al., 2012), as seen in Figure 9a. Other parameters controlling the rates of strength deterioration (C_S), post-capping strength deterioration (C_C), accelerated reloading stiffness (C_A) and unloading stiffness deterioration (C_K) are set at their default values of 1. A sample monotonic backbone and the corresponding hysteretic response of an idealized SDOF model is shown in Figure 9b. The material models used capture in-cycle strength and stiffness degradation. Therefore, the hysteretic behaviour of the system results in lower response than the monotonic backbone. The four different sets of SDOF models represent variations in strength and ductility, from low strength-low ductility (e.g., NBCC 1965) to high strength-high ductility (e.g., NBCC 2015).

Table 3. Key monotonic backbone curve parameters for each idealized system that characterize the strength and ductility of different code eras and building periods.

NBCC	Period (s)	Parameters					
		δ_y (mm)	F_y (kN)	δ_u (mm)	F_u (kN)	δ_r (mm)	F_r (kN)
1965	1	13	231	20	237	46	46
	2	34	303	51	310	121	61
	3	57	338	86	346	202	68
	4	81	358	121	367	286	72
	5	105	372	157	381	372	74
1985	1	18	322	27	330	64	64
	2	51	455	77	466	182	91
	3	94	557	141	571	334	111
	4	145	644	217	660	514	129
	5	203	719	304	737	719	144
1995	1	24	430	97	495	375	86
	2	69	609	274	700	1062	122
	3	126	745	503	857	1951	149
	4	194	861	775	990	3004	172
	5	271	962	1083	1107	4198	192
2015	1	27	475	107	546	414	95
	2	69	611	275	702	1066	122
	3	141	832	562	957	2179	167
	4	203	900	811	1035	3142	180
	5	209	741	834	852	3234	148

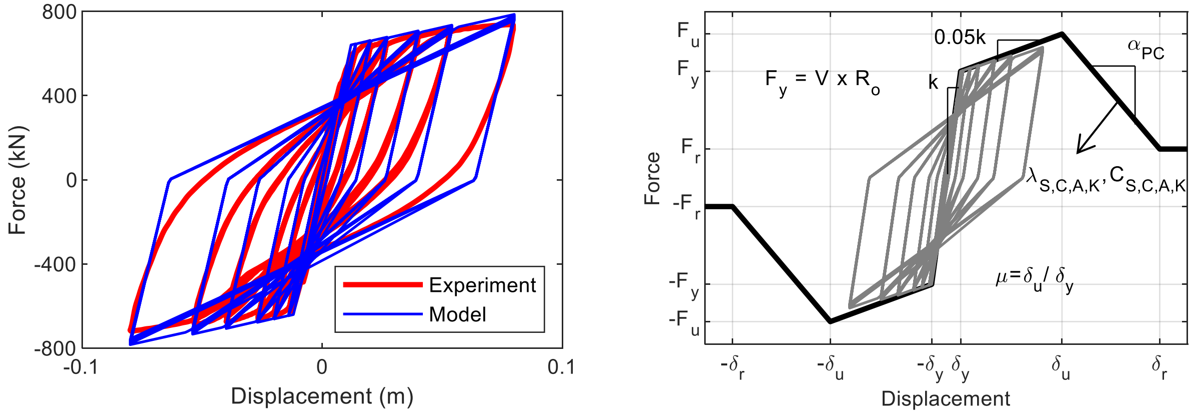

(a) (b)

Figure 9. Idealized reinforced concrete shear wall models: (a) sample calibration illustrating analytical vs experimental results, and (b) generalized monotonic backbone curve showcasing key modeling parameters.

NBCC 2015 Ground Motion Selection

To benchmark building performance under the simulated M9 scenarios against probabilistic estimates of the seismic hazard, which include crustal, intraslab and interface earthquake sources, building response is evaluated with ground motion suites with shaking intensities corresponding to return periods of 100, 475, 975, and 2475-year (or 40%, 10%, 5% and 2% probability of exceedance in 50-years) per CSHM 2015. Ground motions were linearly scaled to match the target UHS at each intensity level considered. The ground motion selection procedure outlined in NBCC 2015 was adopted. The selection procedure requires three distinct suites of 11 ground motion pairs at each intensity level, one per seismic source: crustal, instraslab and interface. NBCC also defines a source-dependent period range for matching. Figure 10 illustrates the resulting ground motions selected to represent the 2% in 50-year probabilistic estimate of the hazard. Ground motions were linearly scaled to match the target over the period range of interest. As observed in Figure 10, the average ground motion suite falls within 90% of the target spectrum over the period range of interest, as required by NBCC 2015. Crustal records were selected using the PEER NGA-West 2 (Ancheta et al., 2014). Intraslab records were selected from the NGA-Subduction (intraslab only) (Ahdi et al., 2017) and S2GM database (Bebamzadeh et al., 2015). Interface records were selected from the K-Net and Kik-NET databases (NIED, 2018), as well as from the S2GM database (Bebamzadeh et al., 2015). The scale factors applied to the 2% in 50 year ground motion suites to obtain the 5%, 10% and 40% in 50-year records are 0.85, 0.6 and 0.24 respectively.

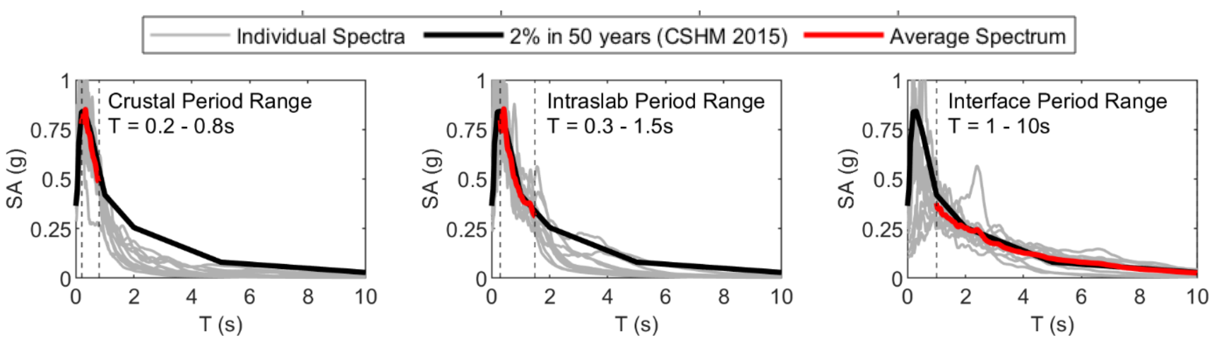

(a) (b) (c)

Figure 10. 2% in 50-year target spectrum, individual ground motion spectra and suite average for (a) crustal, (b) intraslab, and (c) interface selected per NBCC 2015 requirements.

Due to the geographical proximity of the sites of interest considered, as well as the assumption of a uniform site class across all sites, the target UHS for all hazard levels considered are nearly identical. This can be observed in Figure 11, where site-specific spectral acceleration estimates with a 475-year return period for locations A through G are effectively constant. Because of this uniformity in spectral acceleration values across sites, the same ground motion suites, representative of different CSHM 2015 seismic hazard levels, are used. This uniformity in probabilistic estimates of the hazard is in stark contrast to the M9 simulations, which as seen in Figure 11, fluctuate significantly across sites and diverge greatly from the 475-year probabilistic estimates of the hazard.

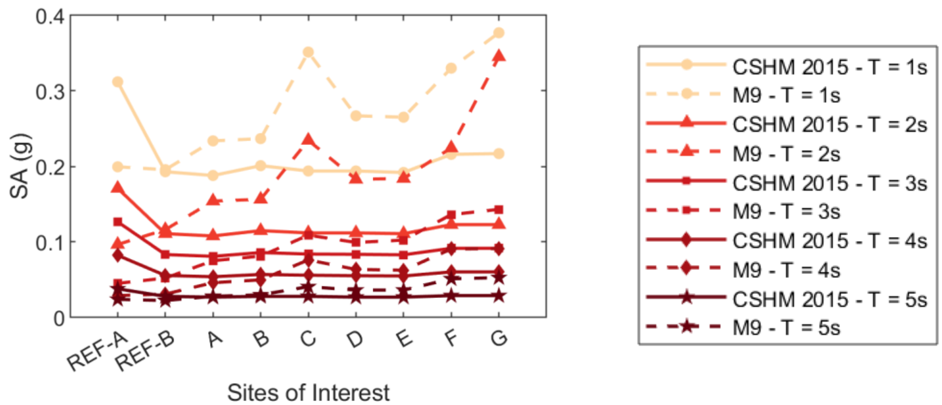

Figure 11. Comparison of 475-year hazard level spectral acceleration CSHM 2015 estimates and average of simulated M9 ground motions at a range of locations and periods of interest.

DUCTILITY DEMANDS AND COLLAPSE RISK

Figure 12 shows the median ductility demand for the idealized systems considered, grouped per code era, when subjected to the simulated M9 ground motions, at different sites throughout Metro Vancouver, and ground motion suites consistent with a 2%, 5% and 10% probability of exceedance in 50 years. Results under the 40% in 50-year hazard level are not shown because they all result in linear elastic response. Collapse is denoted when 50% or more of the ground motions in a given suite result in structural collapse, which is assumed to occur when the lateral displacement of the SDOF models, due to p-delta effects and component deterioration, causes dynamic instability. This dynamic instability occurs when the lateral displacement of the structure increases without bounds. The horizontal dashed line in Figure 12 shows the design ductility level (μ_{Design}), which is defined as the ratio between the ultimate displacement and the yield displacement (see Figure 9b). Ductility demands are calculated as the ratio of the maximum displacement response to the yield displacement. Post-capping degradation and residual strength allow the models to reach displacements beyond the capping point, which can result in ductility demands that exceed the design ductility prior to collapse. However, ductility demands beyond the design level are representative of systems that experience significant levels of strength and stiffness degradation. The shaded areas in Figure 12 represent envelopes of median M9 ductility demand across the sites of interest considered, as reported in Table 1.

The observed ductility demands in all models are higher for shorter periods, for both simulated M9 ground motions and records selected to represent probabilistic estimates of the hazard. Idealized NBCC 1965 systems result in at least 50% probability of collapse conditioned on the occurrence of the M9 simulations for all periods in at least one of the locations considered, typically with larger basin depths. Similarly, idealized NBCC 1985 systems result in at least 50% probability of collapse conditioned on the occurrence of the M9 simulations for periods of 1 and 2-seconds at deep basin sites, while ductility demands exceed the 2475-year hazard at longer periods. Lower bound M9 ductility demands for NBCC 1995 and 2015 systems coincide with demands associated with probabilistic estimates of the hazard with a 975-year return period, whereas upper bound demands generally exceed the 2475-year hazard level estimates. Exceedance of ductility demands above those associated with the 2475-year hazard level, which occur at the deepest basin sites, are of concern because the estimated return period of the M9 ground motions is approximately 500 years (Atwater and Hemphill-Haley, 1997). These trends are consistent with those reported in Figure 3, which benchmark the spectra of the simulated M9 motions against probabilistic estimates of the hazard as well as relevant GMMs, and highlight that Canada's seismic hazard model underestimates seismic demands in basin sites.

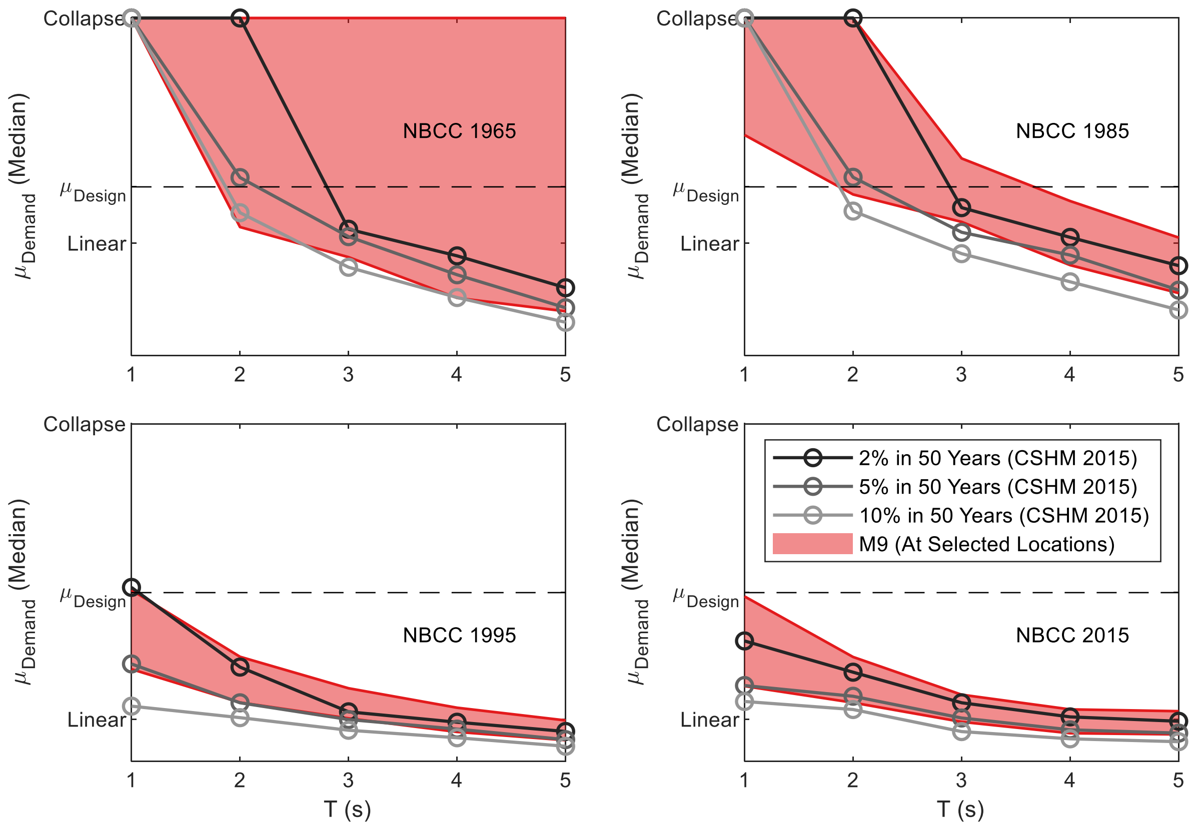

Figure 12. Median ductility demands of idealized RCSW systems of different periods and code eras conditioned on the occurrence of the M9 simulations, at different sites throughout Metro Vancouver, and ground motion suites consistent with a 2%, 5% and 10% probability of exceedance in 50 years. The dashed horizontal lines represent the design ductility level.

When calculating the probability of collapse conditioned on the occurrence of a particular ground motion shaking intensity, the relative contribution of different seismic sources to the overall hazard must be considered. This calculation was carried out as illustrated in Eq. 6, where β_{crustal}, $\beta_{\text{intraslab}}$ and $\beta_{\text{interface}}$ represent the relative contribution to the hazard of each source at a particular period and hazard level, as obtained from seismic hazard deaggregation (Halchuk et al., 2019). Similarly, $P_{\text{C|crustal}}$, $P_{\text{C|intraslab}}$ and $P_{\text{C|interface}}$ are the probabilities of collapse conditioned on the occurrence of ground motion suites representative of crustal, intraslab and interface sources. Table 4 illustrates the relative contribution of each source mechanism (crustal, interface and intraslab) per CSHM 2015. Deaggregation results indicate that at higher shaking intensities and longer periods, the interface earthquake contribution to the total hazard is greatest, reaching values as high as 87% for the 2% in 50-year hazard level (2475-year return period), at a 5-second period. Figure 13 summarizes the probabilities of collapse conditioned on the occurrence of ground motion shaking with a 2%, 5% and 10% probability of exceedance in 50 years, as well as the collapse risk conditioned on the occurrence of the M9 scenarios at different locations throughout Metro Vancouver.

$$P_C = \beta_{\text{crustal}} \times P_{\text{C|crustal}} + \beta_{\text{intraslab}} \times P_{\text{C|intraslab}} + \beta_{\text{interface}} \times P_{\text{C|interface}} \tag{6}$$

Figure 13 highlights a significant collapse risk for NBCC 1965 idealized systems, conditioned on the occurrence of the M9 scenarios, across sites and periods, with an average probability of collapse of 48%. The M9 conditional collapse risk for NBCC 1985 designs are drastically lower at longer periods, i.e., 4-5 s, reaching maximum conditional probabilities of collapse of 24% at the deepest basin site. However, M9 conditional collapse risks are still significant for systems in the 1-3 s period range, with average probabilities of collapse, across sites of 40%. The M9 conditional collapse risk for NBCC 1995 and 2015 designs are drastically lower, reaching peak values at the deepest basin sites of 22% and 15%, respectively. While collapse risk estimates conditioned on the occurrence of the simulated M9 motions vary across code eras, sites and periods, they are generally bounded by collapse risks conditioned on the 975-

year and 2475-year probabilistic estimates of the hazard. The maximum 2% in 50-year conditional collapse risk of NBCC 2015 designs is 5%, which aligns with modern design requirements which target probabilities of collapse of 10% or less at ground motion shaking intensities with a ~2475-year return period (ASCE, 2016).

Table 4. CSHM 2015 percentage contribution of each source mechanism (crustal, interface and intraslab) at each period and intensity level considered in the assessment.

Hazard Level	Source Mechanism	Period (s)				
		1	2	3	4	5
2% in 50 Year	Crustal	11.69	14.34	12.42	10.50	8.57
	Intraslab	50.00	30.40	21.75	13.09	4.44
	Interface	38.31	55.25	65.83	76.41	87.00
5% in 50 Year	Crustal	20.83	13.72	12.12	10.51	8.91
	Intraslab	43.88	37.54	28.84	20.14	11.44
	Interface	35.29	48.74	59.04	69.35	79.66
10% in 50 Year	Crustal	16.58	13.33	11.91	10.50	9.07
	Intraslab	52.48	44.75	38.19	31.63	25.08
	Interface	30.94	41.92	49.90	57.87	65.85
40% in 50 Year	Crustal	15.02	10.77	9.56	8.34	7.38
	Intraslab	64.34	63.35	62.14	60.93	59.47
	Interface	20.64	25.88	28.30	30.73	33.15

While not as intuitive as the results of a scenario-based (e.g., M9 CSZ earthquake) or an intensity-based assessment (e.g., 2% in 50-year hazard), annualized collapse metrics are useful for risk management and recovery planning. In the US, modern building codes (ASCE, 2016) target a maximum collapse risk of 1% in 50 years for determining design spectral accelerations. By fitting a lognormal distribution to the conditional probabilities of collapse at each intensity level considered in the assessment, and integrating the resulting collapse fragility with the corresponding seismic hazard curve, the annualized collapse risk for each idealized RCSW system is evaluated. These collapse risk estimates are also assessed using a hybrid seismic hazard model, which includes both empirical and simulated seismic hazard characterizations. The hybrid hazard model is based on CSHM 2015, but utilizes simulations to represent the large interface earthquake portion of the hazard and empirical relationships for all other earthquake sources (crustal and intraslab). The portion of the collapse risk attributable to interface earthquakes is recomputed using the simulated M9 CSZ scenarios. The annual rate of collapse from the suite of simulated M9 earthquakes is computed as the product of the annual rate for an M9 CSZ earthquake (i.e., reciprocal of the earthquake return period) and the probability of collapse of the archetype building conditioned on the occurrence of the M9 earthquake scenarios considered. More details on this methodology can be found in Molina Hutt et al. (2020). Assuming a Poisson distribution, the probabilities of collapse in 50 years is computed for both the probabilistic and the hybrid seismic hazard models. Table 5 shows the resulting probabilities of collapse in 50 years of the idealized systems for the site within the basin with highest $Z_{2.5}$ values, i.e., Delta.

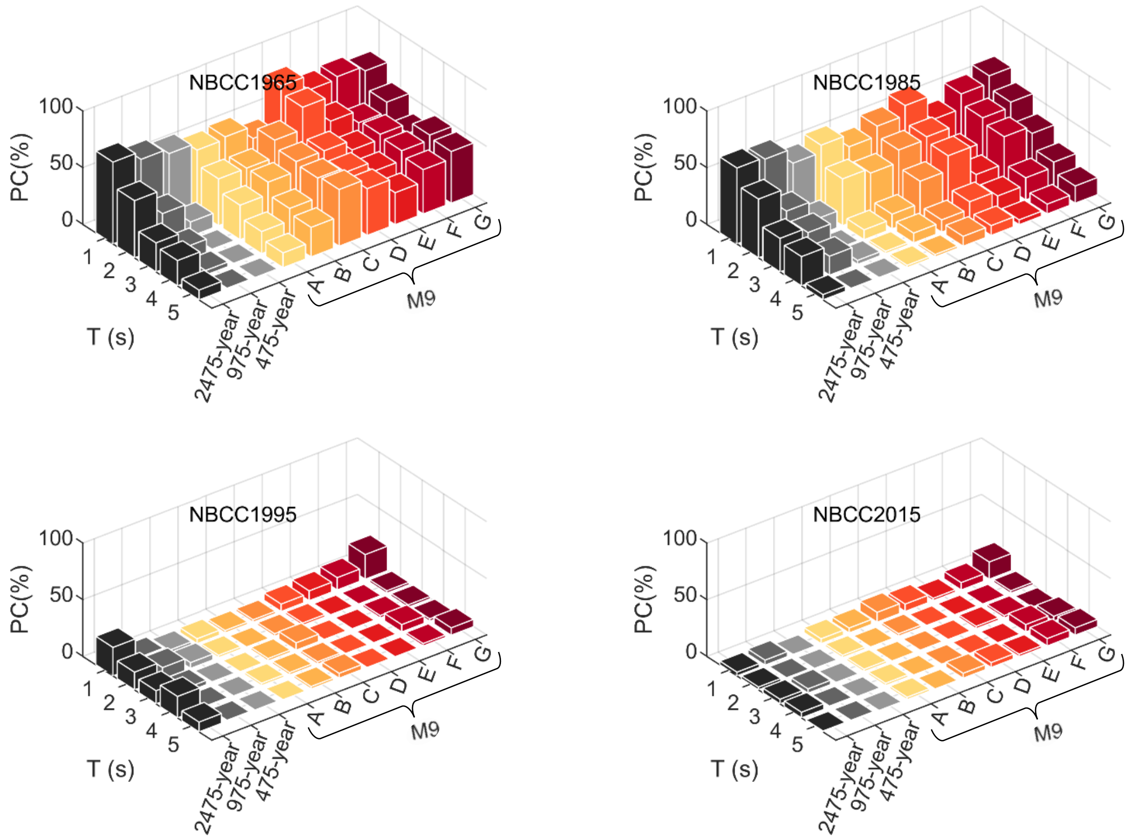

Figure 13. Probability of collapse (PC) of idealized RCSW systems of different periods and code eras conditioned on the occurrence of the M9 simulations, at different sites throughout Metro Vancouver, and ground motion suites consistent with a 2%, 5% and 10% probability of exceedance in 50 years.

As observed in Table 5, the probabilities of collapse predicted by the hybrid seismic hazard model generally exceed those from the probabilistic model. These results further emphasize that Canada's 2015 seismic hazard model underestimates the interface earthquake contribution to the hazard and the associated Georgia basin amplification. Annualized collapse risk estimates in NBCC 1965 and 1985 designs greatly exceed modern targets, particularly for structures with periods of 1-3 s, e.g., NBCC 1965 designs with a 1-second period showcase a twenty-fold increase on the 1% in 50-year collapse risk target implicit in modern design standards. Collapse risk estimates for modern designs, i.e., NBCC 2015, are well in conformance with the collapse risk target of modern codes according to the probabilistic model. However, this threshold is exceeded with explicit consideration of the simulated M9 ground motions and basin amplification for structures with a 1-second period. Similar trends are observed for other sites within the Georgia sedimentary basin.

Table 5. Percent probability of collapse in 50 years using empirical and simulated seismic hazard characterizations at Delta site.

T (s)	NBCC 1965		NBCC 1985		NBCC 1995		NBCC 2015	
	Probabilistic Model	Hybrid Model	Probabilistic Model	Hybrid Model	Probabilistic Model	Hybrid Model	Probabilistic Model	Hybrid Model
1	18.7	19.2	16.1	16.8	2.6	3.4	0.3	1.3
2	6.0	6.8	6.6	7.1	2.6	2.1	0.1	0.3
3	2.0	3.7	2.7	3.8	0.9	0.7	0.3	0.1
4	1.5	4.3	2.7	3.0	0.9	0.7	0.2	0.4
5	0.9	3.9	0.7	1.7	0.6	0.8	0.1	0.5

CONCLUSIONS

By leveraging a suite of simulations of M9 Cascadia Subduction Zone (CSZ) earthquakes, which explicitly account for basin effects for periods greater than 1-second, this study highlights that Canada's current national seismic hazard model (CSHM 2015), adopted by the National Building Code of Canada (NBCC) 2015, underestimates expected ground motion shaking because it does not explicitly consider amplification effects from the Georgia sedimentary basin. To address this issue, this study proposes site-specific and period-dependent spectral acceleration basin amplification factors (*BAF*) throughout the Metro Vancouver region. Ductility demands and probabilities of collapse are evaluated for idealized reinforced concrete shear wall systems representative of different code eras (NBCC 1965, 1985, 1995 and 2015) and building heights (with periods of 1-5 s) at a range of locations. These parameters are also benchmarked against probabilistic estimates of the hazard. A hybrid seismic hazard model that uses empirical and simulated seismic hazard characterizations is also used to estimate the annualized collapse risk of these buildings with explicit consideration of the basin amplification. Key findings are as follows:

- Computed spectral acceleration *BAFs* correlate well with depth to soils with shear wave velocities of 2.5 km/s or $Z_{2.5}$, a proxy commonly used for basin depth. Within Metro Vancouver, the average *BAF* for locations with $Z_{2.5}$ in the range of 1-2 km is 1.72, at a 2-second period, and 2.63 for sites with $Z_{2.5}$ in the range of 3-4 km, at the same period, in relation to a reference site immediately outside the basin.
- Ductility demands from the simulated M9 ground motions were found to exceed those associated with ground motions with 975-year and 2475-year return period shaking intensities, far exceeding the ~500-year return period for large magnitude CSZ earthquakes. While M9 ductility demands vary depending on the site, period and code era, higher ductility demands are observed at deeper basin sites and are most prominent for buildings in the 1-3 s period range.
- Across the sites considered, average probabilities of collapse conditioned on the occurrence of the simulated M9 ground motions for NBCC 1965 and 1985 designs, with 1-second period, are 61% and 53%, respectively. These estimates reduce to 8% and 7% for NBCC 1995 and 2015 designs, respectively. While collapse risk estimates conditioned on the occurrence of the simulated M9 motions vary across code eras, sites and periods, they are generally bounded, at any given site, by collapse risks conditioned on the occurrence of the 975-year and 2475-year return period shaking intensities.
- A hybrid seismic hazard model, which is based on CSHM 2015 and utilizes physics-based simulations to represent the large interface earthquake portion of the hazard and empirical relationships for all other earthquake sources (crustal and intraslab), resulted in an average 56% increase in annualized collapse risk estimates for all buildings and locations considered.

ACKNOWLEDGEMENTS

This research was funded by Canada's Natural Sciences and Engineering Research Council under Discovery Grant No. RGPIN-2019-04599, as well as Canada's New Frontiers in Research Fund – Exploration under Grant No. NFRFE-2018-01060. The authors would also like to thank the University of British Columbia's Cascadia Engagement Fund for supporting this collaboration with the University of Washington. The authors are very grateful to the M9 team at the University of Washington for sharing the results of their M9 simulations in southwest British Columbia, particularly Nasser A. Marafi, Marc O. Eberhard, Jeffrey W. Berman, Arthur D. Frankel and Erin A. Wirth. The authors would also like to acknowledge Alireza Eksir Monfared, MASc student at the University of British Columbia, for his support in developing NBCC 2015 consistent ground motion suites for use in this study.

REFERENCES

Aagaard BT, Graves RW, Rodgers A, et al. Ground-motion modeling of hayward fault scenario earthquakes, part II: Simulation of long-period and broadband ground motions. *Bull Seismol Soc Am* 2010;100(6):2945–77.

Abrahamson N, Gregor N, Addo K. BC hydro ground motion prediction equations for subduction earthquakes. *Earthq Spectra* 2016;32(1):23–44.

Adams J, Halchuk S, Allen T, et al. Canada's 5th Generation Seismic Hazard Model, As Prepared For the 2015 National Building Code of Canada. *11th Can Conf Earthq Eng*, 2015, p. 1–11.

Adebar P, Devall R, Mutrie J. Evolution of high-rise buildings in Vancouver, Canada. *J Int Assoc Bridg Struct Eng* 2017;27(1):7–14.

Ahdi S., Ancheta T., Contreras V, et al. NGA-Subduction Site Database. *16th World Conf Earthq Eng*, 2017.

Ancheta TD, Darragh RB, Stewart JP, et al. NGA-West2 database. *Earthq Spectra* 2014;30(3):989–1005.

ARUP. *Seismic Resilience Study: Seismic Risk Assessment and Recommended Resilience Strategy*. ARUP consulting project for the University of British Columbia 2017.

ASCE. Minimum design loads for buildings and other structures. *ASCE/Structural Engineering Institute (SEI)* 7-16, Reston, VA. 2016.

ATC. *San Francisco tall building study*. Applied Technology Council, Redwood City, CA. 2018.

Atwater BF, Hemphill-Haley E. Recurrence Intervals for Great Earthquakes Of the Past 3,500 Years at Northeastern Willapa Bay, Washington. US Geol Surv Pap 1576 1997.

Atwater BF, Nelson AR, Clauge JJ, et al. Summary of Coastal Geologic Evidence for Past Great Earthquakes at the Cascadia Subduction Zone. *Earthq Spectra* 1995;11(1):1–18.

BC Hydro. Probabilistic Seismic Hazard Analysis (PSHA) Model. 2012.

Bebamzadeh A, Ventura CE, Fairhurst M. S2GM: Ground motion selection and scaling database. A*nnu Los Angeles Tall Build Des Counc Meet* Los Angeles, CA, 2015.

Bielak, J., Taborda, R., Olsen, K. B, et al. Verification and validation of high-frequency (f max= 5 Hz) ground motion simulations of the 2014 M 5.1 La Habra, California, earthquake. *AGUFM*, 2016, S33G-04.

Bijelić, N., Lin, T., & Deierlein, G. G. Quantification of the Influence of Deep Basin Effects on Structural Collapse Using SCEC CyberShake Earthquake Ground Motion Simulations. *Earthq Spectra* 2019, 35(4), 1845–1864.

CAC. Concrete Design Handbook - 4th Edition. 2016.

Campbell KW, Bozorgnia Y. NGA-West2 ground motion model for the average horizontal components of PGA, PGV, and 5% damped linear acceleration response spectra. *Earthq Spectra* 2014;30(3):1087–114.

Campillo M, Bard P-Y, Nicollin F, et al. The Mexico Earthquake of September 19, 1985- The Incident Wavefield in Mexico City during the Great Michoacan Earthquake and Its Interaction with the Deep Basin. *Earthq Spectra* 1988; 4(3):591–608.

Chang SW, Frankel AD, Weaver CS. Report on Workshop to Incorporate Basin Response in the Design of Tall Buildings in the Puget Sound Region, Washington : *U.S. Geological Survey*, Open-File Report 2014:28.

Choi Y, Stewart JP, Graves RW. Empirical model for basin effects accounts for basin depth and source location. Bull Seismol Soc Am 2005;95(4):1412–27.

City of Vancouver, Personal Communication,2020.

Day SM, Graves R, Bielak J, et al. Model for basin effects on long-period response spectra in southern California. Earthq Spectra 2008;24(1):257–77.

Emporis. The global provider of building data. Last retrieved March 1, 2020 from www.emporis.com.

England TD., Bustin RM. Architecture of the Georgia Basin Southwestern British Columbia. *Bull Can Petrleum Geol*

1998;46(June):288–320.

Faccioli, E., Vanini, M., Villani, M., et al. Mapping seismic hazard to account for basin amplification effects. 9th *Intern Work on Sei Micr Risk Red*. 2010. 1-8.

Frankel A. Modeling strong-motion recordings of the 2010 Mw 8.8 Maule, Chile, earthquake with high stress-drop subevents and background slip. *Bull Seismol Soc Am* 2017;107(1):372–86.

Frankel A, Stephenson W, Carver D. Sedimentary basin effects in Seattle, Washington: Ground-motion observations and 3D simulations. *Bull Seismol Soc Am* 2009;99(3):1579–611.

Frankel A, Wirth E, Marafi N, Vidale J, Stephenson W. Broadband synthetic seismograms for magnitude 9 earthquakes on the cascadia megathrust based on 3D simulations and stochastic synthetics, Part 1: Methodology and overall results. *Bull Seismol Soc Am* 2018;108(5):2347–69.

Frankel AD, Petersen MD. Cascadia Subduction Zone, Appendix L in The Uniform California Earthquake Rupture Forecast, version 2 (UCERF 2): U.S. Geological Survey Open-File Report 2007- 1437L and California Geological Survey Special Report 203L, 7 p. 2008.

Halchuk S, Adams J, Kolaj M, el al. Deaggregation of seismic hazard for selected Canadian cities. *12th Can Conf Earthq Eng, 2019*, p. 1-9.

Hyndman RD, Rogers GC. Great earthquakes on Canada's west coast: A review. *Can J Earth Sci* 2010;47(5):801–20.

Ibarra LF, Medina RA, Krawinkler H. Hysteretic models that incorporate strength and stiffness deterioration. *Earthq Eng Struct Dyn* 2005;34(12):1489–511. https://doi.org/10.1002/eqe.495.

Journeay J., Dercole F, Mason D, et al. A Profile of Earthquake Risk for the District of North Vancouver, British Columbia. vol. 151. 2015.

Kakoty P, Monfared AE, Hutt CM. Seismic performance of tall buildings designed following non-prescriptive design procedures. *12th Can Conf Earthq Eng*, 2019, p. 1–7.

Kolozvari K, Tran TA, Wallace JW, et al. Modeling of cyclic shear-flexure interaction in reinforced concrete structural walls. *15th World Conf Earthq Eng* 2012.

Kourehpaz P, Molina Hutt C, Marafi N, et al. Estimating Economic Losses of Mid-rise RC Shear Wall Buildings in Sedimentary Basins by Combining Empirical and Simulated Seismic Hazard Characterizations. *Earthq Eng Struct Dyn*. Accepted.

Marafi NA, Eberhard MO, Berman JW, et al. Impacts of Simulated M9 Cascadia Subduction Zone Motions on Idealized Systems. *Earthq Spectra* 2019;35(3):1261–87.

Marafi NA, Eberhard MO, Berman JW, et al. Effects of deep basins on structural collapse during large subduction earthquakes. *Earthq Spectra* 2017;33(3):963–97.

Marafi NA, Personal Communication,2020.

Mitchell D, Paultre P, Tinawi R, et al. Evolution of Seismic Design Provisions in the National Building Code of Canada. *Can J Civil Eng* 2010;37(9):1157-1170.

Molina Hutt C, Almufti I, Willford M, et al. Seismic Loss and Downtime Assessment of Existing Tall Steel-Framed Buildings and Strategies for Increased Resilience. *J Struct Eng* 2016;142(8):1–17.

Molina Hutt C, Rossetto T, Deierlein GG. Comparative risk-based seismic assessment of 1970s vs modern tall steel moment frames. *J Constr Steel Res* 2019;159:598–610.

Molina Hutt C, Zahedimazandarani S, Marafi NA, Berman JW, Eberhard MO. Collapse Risk of Tall Steel Moment-Resisting Frames in Deep Sedimentary Basins during Large Magnitude Subduction Earthquakes. *Eng Struct* 2020;In-Review.

Molnar S, Cassidy JF, Olsen KB, et al. Earthquake ground motion and 3D Georgia basin amplification in Southwest British Columbia: Shallow blind-thrust scenario earthquakes. *Bull Seismol Soc Am* 2014a;104(1):321–35.

Molnar S, Cassidy JF, Olsen KB, et al. Earthquake ground motion and 3D Georgia basin amplification in Southwest British Columbia: Deep Juan de Fuca Plate scenario earthquakes. *Bull Seismol Soc Am* 2014b;104(1):301–20.

Monahan PA. Soil Hazard Map of the Lower Mainland of British Columbia for Assessing the Earthquake Hazard due to Lateral Ground Shaking. 2005.

Morikawa N, Fujiwara H. A New Ground Motion Prediction Equation for Japan Applicable up to M9 Mega-*Earthquake. J Disaster Res* 2013;8(5):878–88.

Moschetti MP, Luco N, Baltay AS, et al. Incorporating Long-Period (T > 1 S) Earthquake Ground Motions From 3-D Simulations in the U . S . National Seismic Hazard Model 2017:1–12.

Natural Resources Canada, Personal Communication, 2019.

NEHRP. NEHRP Recommended Provisions for Seismic Regulations for New Buildings and Other Structures (FEMA 450). NEHRP Consultants joint venture for the National Institute of Building Science, Washington D.C., 2003.

NIED. Natl Res Inst Earth Sci Disaster Resilience,Stong-Motion Seismogr Networks 2018.

NRCC. National Building Code of Canada, Associate Committee on the National Building Code, *National Research Council of Canada*, Ottawa, ON. 2015.

NRCC. National Building Code of Canada, Associate Committee on the National Building Code, *National Research Council of Canada*, Ottawa, ON. 1995.

NRCC. National Building Code of Canada, Associate Committee on the National Building Code, *National Research Council of Canada*, Ottawa, ON. 1985.

NRCC. National Building Code of Canada, Associate Committee on the National Building Code, *National Research Council of Canada*, Ottawa, ON. 1965.

Olsen KB. Site amplification in the Los Angeles basin from three-dimensional modeling of ground motion. *Bull Seismol Soc Am* 2000;90(6).

Stephenson WJ, Reitman NG, Angster SJ. P- and S-wave velocity models incorporating the Cascadia subduction zone for 3D earthquake ground motion simulations—Update for Open-File Report 2007–1348. *USGS Open File Rep* 2017-1152 2017:17.

Thompson M, Wirth EA, Frankel AD, et al. Basin amplification effects in the Puget Lowland, Washington, from strong-motion recordings and 3D simulations. *Bull Seismol Soc Am* 2020;110(2):534–55.

UBC. Uniform Building Code 1935. *International Conference of Building Officials* (ICBO), Long Beach, California. 1935.

VC Structural Dynamics LTD. Citywide Seismic Vulnerability Assessment of The City of Victoria. 2016.

Wirth EA, Chang SW, Frankel AD. 2018 report on incorporating sedimentary basin response into the design of tall buildings in Seattle, Washington: US Geol Surv Open-File Rep 2018a:19.

Wirth EA, Frankel AD, Marafi N, et al. Broadband synthetic seismograms for magnitude 9 earthquakes on the cascadia megathrust based on 3D simulations and stochastic synthetics, Part 2: Rupture parameters and variability. *Bull Seismol Soc Am* 2018b;108(5):2370–88.

Wirth EA, Frankel AD, Vidale JE. Evaluating a kinematic method for generating broadband ground motions for great subduction zone earthquakes: Application to the 2003 M w 8.3 Tokachi-Oki earthquake. *Bull Seismol Soc Am* 2017;107(4):1737–53.

Wirth EA, Vidale JE, Frankel AD, et al. Source-dependent amplification of earthquake ground motions in deep sedimentary basins. *Geophys Res Let* 2019;46:6443-50

Yathon J, Adebar P, Elwood KJ. A detailed inventory of Non-ductile concrete shear wall buildings. *Earthq Spectra* 2017;33(2):605–22.

Zhu M, McKenna F, Scott MH. OpenSeesPy: Python library for the OpenSees finite element framework. *SoftwareX* 2018;7:6–11.